

Contents list available at CBIORE journal website

International Journal of Renewable Energy Development

Journal homepage: https://ijred.cbiore.id



Research Article

Low voltage ride through (LVRT) enhancement of a two-stage gridconnected photovoltaic system based on finite-control-set model predictive control strategy

Ali Gholipour , Mohammad Farhadi-Kangarlu , Yousef Neyshabouri, Vahid Talavat

Faculty of Electrical and Computer Engineering, Urmia University, Urmia, Iran

Abstract. Grid-connected photovoltaic (PV) systems face numerous challenges during grid faults, including fault detection, synchronization, overcurrent protection, fluctuations in DC-link voltage, and compliance with active and reactive power requirements. This paper presents a control strategy based on finite-control set model predictive control (FCS-MPC) to enhance the LVRT capability of these systems. The strategy incorporates a battery energy storage system (BESS) to improve overall performance. Unlike traditional approaches, the proposed method integrates the control of all switches in boost converters, the BSS controller, and the neutral point clamped (NPC) inverter in one controller. It also combines the Maximum Power Point Tracking (MPPT) within a unified multi-objective cost function framework. By utilizing the positive sequence component of the current, this strategy facilitates symmetrical sinusoidal current injection during grid faults, effectively regulates the DC-link voltage, and maintains balanced capacitor voltages in the NPC inverter while avoiding over-current conditions. The BSS plays a key role in energy management by allowing the PV system to continue operating in MPPT mode during grid faults and enabling the storage of excess solar energy during disturbances. This capability ensures compliance with LVRT grid codes by efficiently managing the injection of reactive and active currents into a compromised grid. The proposed method reduces reliance on traditional cascaded hierarchical control loops, enhancing both dynamic response and system robustness during disturbances. The simulation studies carried out in MATLAB/Simulink environment on a 100 kW three-phase grid-connected PV system demonstrate the effectiveness of the proposed approach. The results indicate that the strategy maintains PV system performance at the maximum power point while significantly improving LVRT capability and overall grid stability. According to the simulation results, although in severe grid faults, the negative sequence grid current is kept at less than 1% and the voltage balance of the capacitors in the NPC inverter is maintained accurately. Also, the voltage ripples on the DC-link capacitors are limited to 7% in the fault period. In conclusion, this integrated control strategy effectively addresses the challenges posed by grid faults and enhances the operational efficiency of grid-connected PV systems, thereby contributing to the resilience of renewable energy infrastructures.

Keywords: Low voltage ride-through, Grid-connected NPC inverter, Finite control set model predictive control (FCS-MPC), Positive and negative voltage sequence component extraction, Maximum Power Point Tracking, DC link voltage control, DC link capacitors voltage balancing



@ The authors. Published by CBIORE. This is an open access article under the CC BY-SA license (http://creativecommons.org/licenses/by-sa/4.0/).

Received: 22nd Sept 2024; Revised: 16th Dec 2024; Accepted: 17th January 2025; Available online: 7th March 2025

1. Introduction

Increasing grid integration of renewable energy sources demands advanced control strategies to ensure reliable and stable PV system operation during grid fault conditions (Jacobson *et al.*, 2022). LVRT is a crucial grid code requirement for PV systems, enabling safe and efficient operation during grid voltage drops. Existing methods, however, are limited by energy losses and complex control strategies, highlighting the need for innovative solutions to optimize PV system performance (Djilali *et al.*, 2019; Farrokhabadi *et al.*, 2019; Miret *et al.*, 2012; Nguyena *et al.*, 2023).

As photovoltaic systems connected to the grid rely heavily on power electronic converters which have low thermal inertia (Jalilian *et al.*, 2018), this may challenge network stability and security (Al-Shetwi *et al.*, 2020; Naderi *et al.*, 2018). New grid codes, including LVRT requirements, have been developed to integrate photovoltaic power plants into the power networks. In

the event of a grid fault, the point of common coupling (PCC) voltage may experience a voltage sag. To support the grid, photovoltaic systems must remain connected, posing two challenges. Firstly, the system must protect the inverter from overcurrent while maintaining a grid connection. Secondly, it must inject reactive current to meet grid code requirements (Al-Shetwi & Sujod, 2018). An advanced control strategy enables photovoltaic systems to accurately detect grid phase angle under faults, stay synchronized, and adjust reactive power injection according to grid code. It also ensures the inverter stays within the rated current limits, maintaining DC link voltage and providing balanced currents for healthy and unbalanced phases (Kerekes et al., 2017; Romero-Cadaval et al., 2013).

The identification of the maximum power point (MPP) in PV systems achieved through methods like Perturbation and Observation (P&O), Incremental Conductance (IC), and soft computing techniques, are essential for optimal energy

^{*} Corresponding author Email: m.farhadi@urmia.ac.ir (M. Farhadi-Kangarlu)

production (Omar & Mahmoud, 2021; Singh & Gupta, 2018). This is because the MPP of the PV array changes with variations in irradiance and temperature, which can affect grid stability during LVRT(Alrubaie *et al.*, 2022; Anagreh *et al.*, 2021). In (Chen *et al.*, 2016; Jalilian *et al.*, 2015; Lee *et al.*, 2011; and Sadeghkhani *et al.*, 2016), studies focus on new control strategies or auxiliary circuits to control the inverter current in LVRT conditions and reactive current injection.

In (Haidar & Julai, 2019; Lin et al., 2018; Naresh & Kumar, 2020; RajaMohamed et al., 2019), a local load comprising a resistor and a semiconductor switch is used to mitigate power imbalance issues during grid faults. This solution maintains the photovoltaic system's power generation at MPP, offering simplicity, but also incurs power losses and requires a dynamic load capable of handling the system-rated power. To avoid power loss in the previous methods and improve LVRT, alternative solutions (Afshari et al., 2017; Huka et al., 2018; Mohamed et al., 2019; Nezhad et al., 2017), are presented to remove the operating point of the photovoltaic system from the MPP. By doing so, the power produced can be reduced, which helps to balance the power in the case of a PCC voltage drop. This method includes fault detection and a control scheme called non-MPPT, where the generated power of the photovoltaic system is reduced proportionally to the voltage drop in the PCC (Gulalkari & Chaudhary, 2020).

DC link capacitor voltage control in two-stage photovoltaic systems presented in (Mirhosseini et al., 2014), deviates from the MPP operating. The proposed approach approximates the power-voltage curve to determine the operating point under fault conditions. However, it does not explain the details of inverter behavior and control. Previous studies, such as (Wen & Fazeli, 2019b), have explored single-stage photovoltaic systems with compensating voltages added to the DC link capacitor voltage reference. These methods employ positive- and negative-sequence components of the grid voltages to improve the control system's dynamic response. Another study (Wen & Fazeli, 2019a), utilized the Lyapunov stability criterion and a potential energy function to develop a method for calculating compensating voltages based on grid voltage drops, However, it has drawbacks, including complex control calculations and deviation from the MPP operating condition.

Additional devices, such as Fault Current Limiter (FCL) have been explored to improve LVRT and protect inverters against excess currents. The FCL has been particularly effective in limiting fault currents (Safaei et al., 2020). The application of FCL for improving LVRT has been reported in some works (Asghar et al., 2020; Naderi et al., 2017; Rashid & Ali, 2014). In (Jalilian et al., 2015; Jalilian et al., 2018), the Controllable Diode Bridge Fault Limiter (CD-BFCL) is utilized to limit fault current and enhance LVRT capability. However, approximately 2% of the generated power is lost due to the permanent presence of the diode bridge in the circuit (Abramovitz & Smedley, 2012). In (Alam et al., 2018; Hossain & Ali, 2014), a Series Dynamic Braking Resistor (SDBR) is inserted into the circuit. During normal operation, the semiconductor switch bypasses the resistor, however, when a voltage drop occurs, the switch changes state and the resistor is inserted, limiting the current. This simple method leads to energy loss, while the voltage at the PCC experiences a smaller decrease. Current control strategies employed to enhance LVRT capability lie in their reliability, stability, dynamic response, harmonic compensation, and protection of power electronic devices (Hassan et al., 2020). A study in (Camacho et al., 2014), investigated an active and reactive power control strategy for unbalanced voltage deep grid conditions. The reference currents were separated into active and reactive parts in the stationary reference frame ($\alpha\beta$),

and their positive and negative sequence terms were calculated utilizing the second-order generalized integral technique (SOGI) (Rodriguez *et al.*, 2008). This approach allows for the control of currents within defined ranges, as a significant advantage. However, LVRT conditions under different grid faults and the relevant priorities have not been explored.

In (Castilla et al., 2010; Miret et al., 2012), different current control strategies are compared in terms of their LVRT capability. By fractional changing the values of α and β , a new method is proposed. However, the injected currents in this method have more distortion and are not sinusoidal. However, the peak fault current is well limited. In (Lin et al., 2018), the double synchronous reference frame (DSRF) is utilized to extract the positive and negative sequence of the grid voltage and control the negative-sequence current reference in zero. As a result, the minimum current passes through the inverter during fault conditions. Both the active and reactive power, in addition to their average values, are expected to fluctuate at twice the fundamental frequency. These lead to considerable ripples in the voltage of the DC link capacitor at the twice fundamental frequency. This article ignores the effect of impedance between the inverter and the grid in the current control section. This impedance causes the mutual influence of dq currents on the voltage reference of the inverter.

Other researchers, such as (Huka *et al.*, 2018; Liu & Tian, 2016; Mohamed *et al.*, 2019; Mortazavian *et al.*, 2016; Wang *et al.*, 2014; Zeb *et al.*, 2022), have studied the operation of PV systems grid faults. In the work (Mortazavian *et al.*, 2016), a control compensator is proposed to reduce the initial transient high current after the fault occurs. This paper attempts to move the poles of the control system transfer function to the left side to increase the system stability. This results in an increase in the damping coefficient of the poles with higher frequency, which leads to a decrease in the primary transient current and an increase in LVRT capability. However, there is no reactive power injection to support the grid under fault conditions. Generally speaking, one of the major challenges in the mentioned works, is the several cascaded control loops which degrades the operation of the inverter under AC grid faults.

In this article, a novel control strategy is proposed that simultaneously controls the boost converter and the PV inverter. This novel control strategy is based on finite controlset model predictive control (FCS-MPC) to significantly enhance the low-voltage ride-through capability of the studied grid-connected photovoltaic system. The proposed method selects the optimal switching state from 2×27 possible combinations, taking into account the inverter currents, DC link voltage, voltage balance of the two DC link capacitors, and maximum power point tracking (MPPT) and following LVRT grid codes. All the mentioned objectives are defined within a multi-objective cost function. The algorithm models the boost converter using state equations and predicts the neutral point clamped (NPC) inverter's behavior using discrete-time models, then selects the optimal switching states. The cost function directly controls the boost converter switch state, ensuring the photovoltaic system operates in MPPT mode during lowvoltage conditions, thereby minimizing power losses and ensuring safe operation. During LVRT where the reactive power is injected into the grid, the extra active power absorbed from PV arrays is stored in an energy storage system and after removing grid failure is injected into the grid.

The rest of this article is organized as follows: The structure of the case study is described in section 2. Section 3 elaborates on the proposed LVRT control strategy. In subsection 3. A, the space state model of the boost converter and its discrete-time

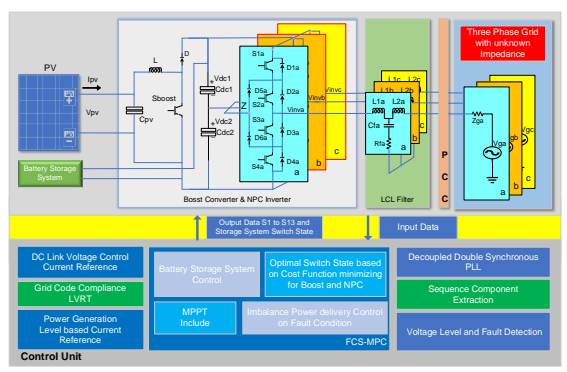


Fig. 1 General block diagram of the two-stage photovoltaic system connected to the AC grid

model are extracted Afterwards, subsection 3. B three-level NPC inverter predictive modeling is performed. Finally, in subsection 3. C a multi-objective cost function including LVRT grid codes, voltage balance of DC link capacitors, limiting fault currents and tracking the maximum power point is developed. In section 4, the simulation results in MATLAB/Simulink environment are provided. Finally, the paper is concluded in section 5.

2. Two-stage grid-connected PV system structure and component modeling

The schematic of a two-stage photovoltaic system, illustrated in Fig. 1, consists of a boost converter and a three-level three-phase NPC inverter(Kerekes *et al.*, 2017; Liu *et al.*, 2019). The system connects to the 3-phase grid at the PCC. The inverter has to maintain a stable connection to the grid during grid fault conditions while meeting LVRT requirements. We propose a novel control strategy to improve the overall functionality of the system in terms of LVRT capability. The control strategy is based on FCS-MPC to select the optimal switching states for the 13 switches in the entire system.

The overall control block diagram of the system has been presented in Fig. 1. This paper models the boost converter using state equations and predicts the NPC inverter's behavior using a predictive model. Then, with the use of a multi-objective cost function, selects the optimal switching state. During fault conditions, the presented method minimizes a cost function to ensure safe operation within the defined limits. Unlike conventional approaches, the proposed strategy does not need cascaded and separated control systems for each part and all control targets are included in a multi-objective MPC system improving the dynamic response of the system. We utilize BESS to store extra energy generated during fault conditions, enhancing system reliability and efficiency. The proposed control enables injecting reactive current based on grid code requirements. The mentioned features improve reliability and efficiency and allow power generation to remain in (MPPT) even during grid fault conditions, ensuring optimal energy harvesting.

3. Proposed LVRT Control Strategy

3.1. Discrete-time Model of a Boost Converter

Fig. 2 depicts a boost converter. To realize model predictive control, the governing state space equations are extracted through the switching state model(Mahmoudi *et al.*, 2017).

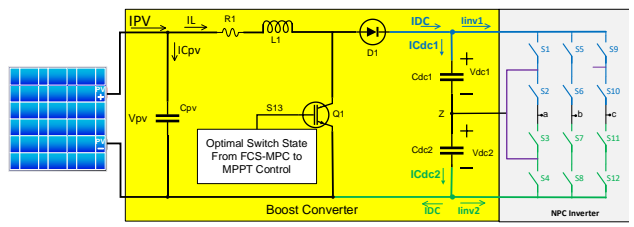


Fig. 2 Boost converter circuit

Assuming that the current flowing through the inductor is greater than zero($I_L>0$) the following equations can be written when the switch is OFF.

$$V_{pv} = R_L I_L + L \frac{dI_L}{dt} + V_{DC1} + V_{DC2}$$
 Switch off $U(t) = 0$ (1)

Where V_{pv} is the PV array output voltage, I_L is the boost converter inductance current, L and R_L are the boost converter inductance and its ohmic resistance, respectively and V_{DC1} and V_{DC2} are the DC link capacitors voltages.

$$I_{DC} = C_{DC1} \frac{dV_{DC1}}{dt} + I_{inv1} = C_{DC2} \frac{dV_{DC2}}{dt} - I_{inv2}$$
 (2)

Where: I_{DC} is the diode current, I_{inv1} and I_{inv2} are the inverter up legs and down legs input current and C_{DC1} and C_{DC2} are DC link capacitance. Also, for a state the switch is ON, we have(Ikaouassen *et al.*, 2019)

$$I_{PV} = C_{PV} * \frac{dV_{PV}}{dt} + I_L \tag{4}$$

Equations 1 to 4 can be arranged in the following order based on the state variables: I_L , V_{DC1} , V_{DC2} , V_{PV} .

$$\begin{cases} I_{DC} = (1-u) * I_{L} & and \ u = 0 \ switch \ off \\ \frac{dI_{L}}{dt} = \frac{V_{PV}}{L} - \frac{R_{L}}{L} I_{L} - \frac{V_{DC1}}{L} - \frac{V_{DC2}}{L} \\ \frac{dV_{DC1}}{dt} = \frac{I_{DC}}{C_{DC1}} - \frac{I_{inv1}}{C_{DC1}} \\ \frac{dV_{DC2}}{dt} = \frac{I_{DC}}{C_{DC2}} + \frac{I_{inv2}}{C_{DC2}} \\ \frac{dV_{PV}}{dt} = \frac{I_{PV}}{C_{PV}} - \frac{I_{L}}{C_{PV}} \end{cases}$$
(5)

where: u is state of the boost converter switch, C_{PV} is the input capacitor be tween PV and the boost converter

$$\begin{cases} I_{DC} = (1-u) * I_L & and \ u = 1 \text{ switch on} \\ \frac{dI_L}{dt} = \frac{V_{PV}}{L} - \frac{R_L}{L} I_L \\ \frac{dV_{DC1}}{dt} = -\frac{I_{Inv1}}{C_{DC1}} \\ \frac{dV_{DC2}}{dt} = + \frac{I_{Inv2}}{C_{DC2}} \\ \frac{dV_{PV}}{dt} = \frac{I_{PV}}{C_{DV}} - \frac{I_L}{C_{DV}} \end{cases}$$

$$(6)$$

The state space equations of (6) can be expressed in the standard form of (7)

$$\begin{cases} x' = A_1 * x + B_1 * U & u(t) = 0 \\ x' = A_2 * x + B_2 * U & u(t) = 1 \end{cases}$$
 (7)

By combining equations (5) and (6), and use of (7), the statespace equations of the boost converter can be written as follows.

$$x' = [A_1 + u * (A_2 - A_1)] * x + B * U, u = 0 \text{ or } 1$$
 (8)

Where the state variables are as follows.

$$x(k) = [I_L(k) \quad V_{DC1}(k) \quad V_{DC2}(k) \quad V_{pv}(k)]^T$$
(9)

From (5) and (6), the matrices of coefficients in (8) are obtained as follows.

for B1 and B2 coefficients as

$$B_1 = B_2 = \begin{bmatrix} 0 & 0 & 0 \\ 0 & -\frac{1}{C_{PV}} & 0 \\ 0 & 0 & \frac{1}{C_{DC_2}} \\ \frac{1}{C_{PV}} & 0 & 0 \end{bmatrix}$$
 (11)

Finally, the discrete-time model of the boost converter is obtained as follows (Lashab *et al.*, 2017).

$$x(k+1) = [I + (A_1 + u * (A_2 - A_1)) * T_s] * x(k) + B_1 * U(k)$$
(12)

Where: I is a 4x4 identity matrix, u is the switch state 0 or 1, T_s is sample time, x(k) is the current variable value, x(k+1) is the next variable value and U(k) can be expressed as follows.

$$U(k) = [I_{PV}(k) \quad I_{inv1}(k) \quad I_{inv2}(k)]^{T}$$
(13)

Where: U(k) is the input matrix, I_{pv} is the output current of the PV panels, I_{inv1} is the input current on the upper side of the inverter and I_{inv2} is the input current on the lower side of the inverter.

3.2. Discrete-time model of the three-level NPC three-phase inverter

The NPC inverter is a commonly used multilevel converter in PV applications (Donoso *et al.*, 2017; Yu *et al.*, 2021). Fig. 3 shows the grid-connected NPC inverter with an LCL filter (Dursun & DÖŞOĞLU, 2018; Jalili & Bernet, 2009). The DC link capacitors are charged by the boost converter. The control system compares the actual capacitor voltage with the reference value. A PI controller is used to determine the active current reference for the NPC inverter

The relation between the input currents of the inverter and a, b and c output currents can be obtained based on the ON and OFF status of the switches which can be written as follows:

$$\begin{cases} I_{inv1}(k) = H1_a * I_{1a}(k) + H1_b * I_{1b}(k) + H1_c * I_{1c}(k) \\ I_{inv2}(k) = H2_a * I_{1a}(k) + H2_b * I_{1b}(k) + H2_c * I_{1c}(k) \end{cases}$$
(14)

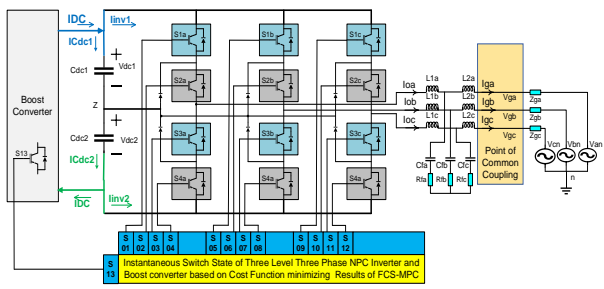


Fig. 3 Detail base model of three-level three-phase neutral point Inverter with LCL filter connected to three-phase grid

Where: $I_{1a}(k)$ is the inverter output current in phase a, $I_{1b}(k)$ is the inverter output current in phase b and $I_{1c}(k)$ is the inverter output current in phase c, and also In (14), H_{1x} and H_{2x} are function of switching states as defined in (15).

$$\begin{cases} H1_{a,b,c} = 1 & if \ S1, S2_{a,b,c} \ on \\ H1_{a,b,c} = 0 & if \ S1, S2_{a,b,c} \ off \\ H2_{a,b,c} = 1 & if \ S3, S4_{a,b,c} \ on \\ H2_{a,b,c} = 0 & if \ S3, S4_{a,b,c} \ off \end{cases}$$

$$(15)$$

The S1, S2, S3 and S4 denote four switches in each phase of the inverter. Additionally, the currents of the DC link capacitors are obtained from (16).

$$\begin{cases}
I_{Cdc1}(k) = I_{DC}(k) - I_{inv1}(k) \\
I_{Cdc2}(k) = I_{DC}(k) + I_{inv2}(k)
\end{cases}$$
(16)

On the other hand, according to (17), turning the boost converter switch ON or OFF affects the I_{DC} as expressed in (17).

$$I_{DC}(k) = (1-u) * I_L , \begin{cases} Switch \ off \ u = 0 \\ Switch \ on \ u = 1 \end{cases}$$
 (17)

Table 1 shows the relationship between the output voltage of the inverter and its input DC voltage, based on the different switching states, where $x \in \{a, b, c\}$. For example, Switch1(a)

Table 1
The NPC converter switching s

The NPC converter switching states					
Phase(X) Switch Number	Switch 1(x)	Switch 2(x)	Switch 3(x)	Switch 4(x)	(X)z voltage
State	0	0	1	1	Vdc2
0 off	0	1	1	0	0
1 on	1	1	0	0	Vdc1

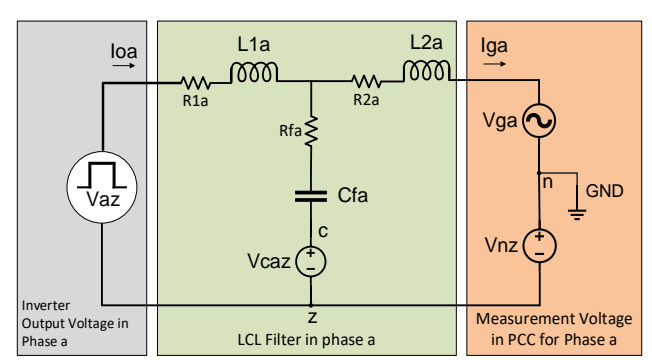


Fig. 4 Equivalent circuit model of one-phase inverter connected to the

and Switch2(a) are two upper leg switches of phase a. If both upper leg switches are turned on, the output of phase a is anticipated to be equal to $V_{\rm dc1}$. There are 27 valid modes for all switches in a three-phase, 3-level NPC. Each phase of the inverter can be modeled according to Fig. 4 (Lim & Choi, 2015; Rossi *et al.*, 2022),

Applying KVL to the circuit model of Fig. 4, the equation (18) is obtained.

$$V_{az} = R_{f1} * I_{oa} + L_{f1} * \frac{dI_{oa}}{dt} + R_{f2} * I_{ga} + L_{f2} * \frac{dI_{ga}}{dt} + V_{ga} + V_{nz}$$
(18)

Where: V_{az} is the output voltage of the inverter in phase a with respect to the neutral point z, I_{oa} is the output current of the inverter in phase a, I_{ga} is the output current of the LCL filter to the grid at PCC, R_{f1} is the resistance of the filter on the inverter side, L_{f1} is the inverter side inductor filter, R_{f2} is the resistance of the LCL inductor filter on the grid side, L_{f2} is the filter inductor on the grid side, V_{ga} is the measured voltage of phase a of the grid at PCC and V_{nz} is the common-mode voltage obtained from (19).

$$V_{nz}(k) = \frac{(V_{az}(k) + V_{bz}(k) + V_{cz}(k))}{3}$$
 (19)

There are several discretization methods available to discretize the continuous-time equations. In this article, Euler's forward and backward discretization methods are used, as expressed in equation (20) (Monfared *et al.*, 2022).

$$\frac{dx}{dt} \cong \frac{\left(x(k+1) - x(k)\right)}{T_s} \cong \frac{\left(x(k) - x(k-1)\right)}{T_s} \tag{20}$$

In (20), x stands for the voltage or current and Ts represents the sampling time. Applying (20) to (18) and (19), the following relation is obtained.

$$R_{f1} * I_{oa}(k) + L_{f1} * \frac{\left(I_{oa}(k+1) - I_{oa}(k)\right)}{T_s} + R_{f2} * I_{ga}(k) + L_{f2} * \frac{\left(I_{ga}(k) - I_{ga}(k-1)\right)}{T_s} = V_{az}(k) - V_{ga} - \frac{\left(V_{ga}(k) + V_{gb}(k) + V_{gc}(k)\right)}{3}$$
(21)

Finally, equation (22) can be derived from (21), which depicts the predictive current of phase a.

$$\begin{split} I_{oa}(k+1) &= \left(1 - \frac{R_{f1}T_s}{L_{f1}}\right) * I_{oa}(k) - \left(\frac{R_{f2}T_s}{L_{f1}} + \frac{L_{f2}}{L_{f1}}\right) * \\ I_{ga}(k) &+ \frac{L_{f2}}{L_{f1}} * I_{ga}(k-1) + \frac{T_s}{3L_{f1}} * \left(2V_{az}(k) - V_{bz}(k) - V_{cz}(k) - 3V_{ga}(k)\right) \end{split} \tag{22}$$

$$\begin{cases} I_{ob}(k+1) = \left(1 - \frac{R_{f1}T_s}{L_{f1}}\right) * I_{ob}(k) - \left(\frac{R_{f2}T_s}{L_{f1}} + \frac{L_{f2}}{L_{f1}}\right) * I_{gb}(k) \\ + \frac{L_{f2}}{L_{f1}}I_{gb}(k-1) \\ + \frac{T_s}{3L_{f1}} * \left(2V_{az}(k) - V_{bz}(k) - V_{cz}(k) - 3V_{gb}(k)\right) \\ I_{oc}(k+1) = \left(1 - \frac{R_{f1}T_s}{L_{f1}}\right) * I_{oc}(k) - \left(\frac{R_{f2}T_s}{L_{f1}} + \frac{L_{f2}}{L_{f1}}\right) * I_{gc}(k) \\ + \frac{L_{f2}}{L_{f1}} * I_{gc}(k-1) \\ + \frac{T_s}{3L_{f1}} * \left(2V_{az}(k) - V_{bz}(k) - V_{cz}(k) - 3V_{gc}(k)\right) \end{cases}$$
(23)

In the given relationship, k represents the current sample, and k+1 represents the next sample, which is used to predict the system behavior. Similarly, for phases b and c, the same predictive current relations are obtained as noted in (23).

3.3. Multi-objective model predictive control-based strategy for enhanced LVRT capability

In this article, a novel control strategy based on FCS-MPC is proposed that aims to integrate the inverter model with the boost converter model to achieve the optimal prediction through a multi-objective cost function. Traditionally, extracting the maximum power from PV is achieved by controlling the duty cycle of the boost converter. Various methods have been developed for this purpose, such as the perturbation and observation method (Abdelsalam et al., 2011; Alrubaie et al., 2022), and the incremental conduction method (Alrubaie et al., 2022; Liu et al., 2022; Mahmoudi et al., 2017; Pant & Saini, 2019). This article proposes a method that performs MMPT in combination with the inverter control that is all combined in an FCS-MPC based control strategy. During grid fault, the proposed method provides a faster dynamic response to mitigate fault current, inject reactive current to the grid according to LVRT codes and maintain balanced capacitors voltages in the NPC inverter.

Although synchronization with the grid is commonly achieved in three-phase systems using the SRF-PLL (Teodorescu *et al.*, 2011), it does not provide a suitable dynamic response in the presence of asymmetrical voltage sags caused by asymmetrical grid faults at the PCC (Rodriguez *et al.*, 2011; Teodorescu *et al.*, 2011). In this article, the decoupled double synchronous reference frame phase-locked loop (DDSRF-PLL) (Rodriguez *et al.*, 2007; Teodorescu *et al.*, 2011) is utilized to separate the positive and negative sequences components of the voltage and current. Under normal operating conditions, only the positive-sequence active current is injected into the grid. This active current controls the DC link voltage, enabling the transfer of active input power from the inverter to the grid. Fig. 5 depicts the block diagram for determination of the active current reference.

In Fig. 5, V_{dcref} represents the DC link reference voltage, while V_{dcm} represents its measured value obtained from the sum of the two capacitors' DC-link voltages. With the help of the PI controller, the positive sequence term of the active current is determined. This allows the input power to be transferred from the boost converter to the grid through the inverter. In the Park transformation, the θ is used for the positive sequence extraction, while the $-\theta$ angle is used for the negative sequence extraction that is obtained from DDSRF-PLL. To investigate the behavior of the system under unbalanced grid conditions caused by grid faults, this article considers the requirements of the German grid code as a reference (Al-Shetwi & Sujod, 2018; Troester, 2009). Therefore, reactive current is predicted to be injected into the grid according to the drop in accordance with the drop in the positive sequence of the grid voltage. Subsequently, the active current injection is to be implemented as the second priority. The total currents should not exceed the rated current of the inverter. Eq. (24) shows the reactive current injection in terms of voltage changes, in accordance with the German grid code (Mirhosseini et al., 2014; Sadeghkhani et al., 2018; Zeb et al., 2022),

$$I_{q} = \begin{cases} I_{q0} & 0.9 \ p.u \le V \le 1.1 \ p.u \\ K * \frac{V - V_{0}}{V_{N}} * I_{N} & 0.5 \ p.u \le V < 0.9 \ p.u \\ I_{N} & V \le 0.5 \ p.u \end{cases}$$
(24)

Where: K is the constant coefficient. V_0 represents the primary voltage, V represents the space vector voltage of the grid, V_N represents the nominal voltage of the grid, I_N is the nominal effective current, and I_{q0} is the injected reactive current before the fault.

At each moment, the voltage at the PCC is measured and the positive and negative sequence components of voltage are extracted. To calculate the space vector V_S in the presence of positive and negative sequence components, the following relationship is employed (Teodorescu *et al.*, 2011),

$$|Vs| = \sqrt{(VP)^2 + (VN)^2 + 2VP.VN.\cos(2\omega t + \theta pn)}$$
 (25)

Where: V_P and V_N represent the space vector of the positive and negative sequence magnitudes, respectively. Also, the ω t represents the angle of the grid voltage, θ pn is the angle

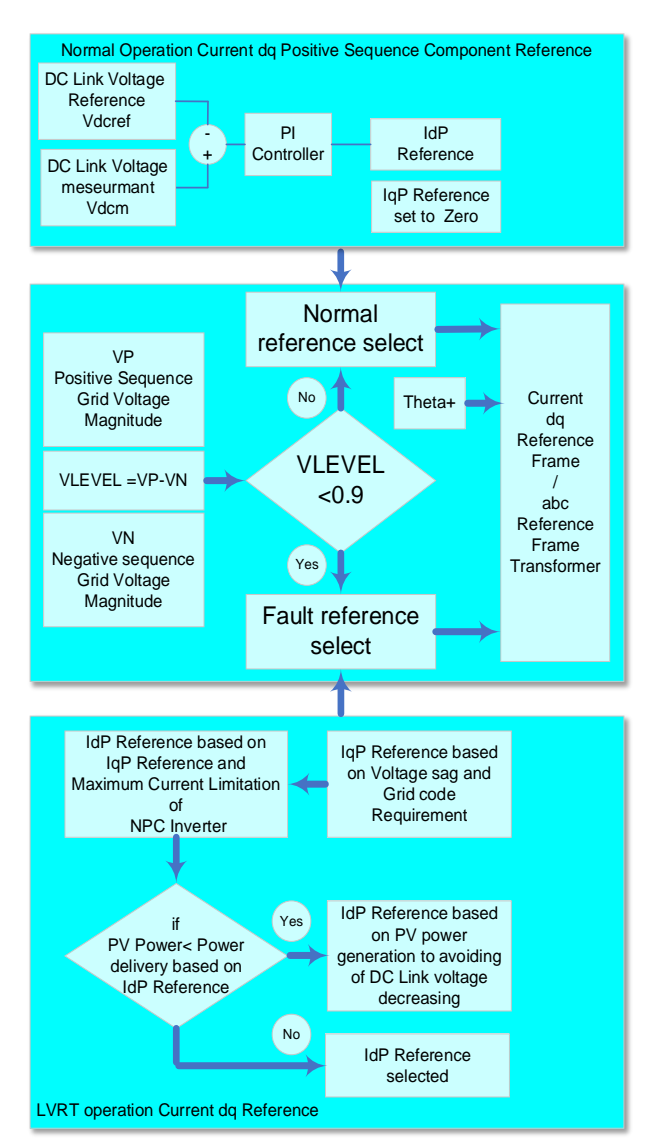


Fig. 5 Block diagram of active and reactive current reference generation of the inverter

between positive and negative sequence components and $V_{\rm S}$ is the space vector of the grid voltage at the PCC. The voltage level is determined based on its minimum value (Huka *et al.*, 2018). In this article, the minimum value of the above relationship is used to detect voltage sag faults. Therefore,

$$|Vs| = V^+ - V^- \tag{26}$$

If Vs is less than 0.9 per unit, it indicates the presence of a fault in the grid. The reactive current reference is then selected according to Eq. (24), followed by the selection of the active current I_a ⁺ based on Eq. (27) (Yang *et al.*, 2015),

$$I_d^+ = \left(\sqrt{\left(1 - I_q^{+2}\right)}\right) * I_N$$
 (27)

Consequently, the active transmission power from the inverter in the corresponding positive component is obtained from Eq. (28).

$$P^{+} = \frac{3}{2} V_{d}^{+} * I_{d}^{+} \tag{28}$$

It is assumed that, with the help of the control strategy, the transmitted power caused by the negative-sequence components is set to zero. In situations where the generated power of the panels exceeds the power obtained from Eq. (28), the voltage of the DC link increases. To prevent such an overvoltage, a battery is connected to the DC link through a buck converter to absorb the extra energy of the panels. On the other hand, if the output power of the panels is lower than the active power value of relation (28) due to factors such as reduced radiation intensity, the active current reference of Eq. (27) is replaced with Eq. (29) to maintain the voltage of the DC link and prevent its drop.

$$I_d^+ = \frac{2*(V_{PV}*I_{PV})}{3V_d^+} \tag{29}$$

Where: V_d^+ is a positive sequence of PCC voltage. After determining the reference active and reactive currents, the multi-objective cost function is defined as (30).

$$f_{cost} = (\lambda_{1} * |Ppvm - Ppv(k)|) + (\lambda_{2} * |I_{pv}(k+1) - I_{pv}(k)|) + (\lambda_{3} * |I_{oa}(k+1) - I_{refa}|) + (\lambda_{3} * |I_{ob}(k+1) - I_{refb}|) + (\lambda_{3} * |I_{oc}(k+1) - I_{refc}|) + (\lambda_{4} * |V_{dc1}(k+1) - V_{dc2}(k+1)|)$$
(30)

Where: P_{pvm} is predictive PV power, $P_{pv}(k)$ is PV power in current sample, $I_{pv}(k)$ and $I_{pv}(k+1)$ are PV current in current and next time value respectively, $I_{o(a,b,c)}(k+1)$ are predictive current of each phase of three-phase inverter obtained by algorithm, $I_{ref(a,b,c)}$ are reference current that calculated by control unit using I_{d}^{+} and I_{q}^{+} obtained of Eq. (24), Eq. (27) and Eq.(29) and $\lambda_{(1,2,...,4)}$ are the weighting factors,

The multi-objective cost function of Eq. (30) aims to balance the DC link capacitors' voltages and select the optimal state of the switches to follow the reference currents at the inverter output and also aim to reach MPPT. To minimize the cost function, the state of the inverter switches and as well as the boost converter switch are determined using the proposed algorithm shown in Fig. 6. It can be seen that in the proposed strategy, MPPT is combined with inverter current control

through the developed FCS-MPC based LVRT strategy. The weighting factors, λ are chosen empirically in this article.

4. Simulation results and discussion

To validate the proposed control strategy, a 100 [kW] PV system is simulated in MATLAB/Simulink software. The case study parameters are given in Table 2. It is assumed that the

grid is strong, meaning that the grid inductance is negligible compared to the filter inductance (Xu et al., 2013)

4.1 Low voltage ride through under symmetric three-phase grid fault

The Photovoltaic system generates 100 kilowatts of power in nominal operation. The DC link voltage is set to 500 V and the

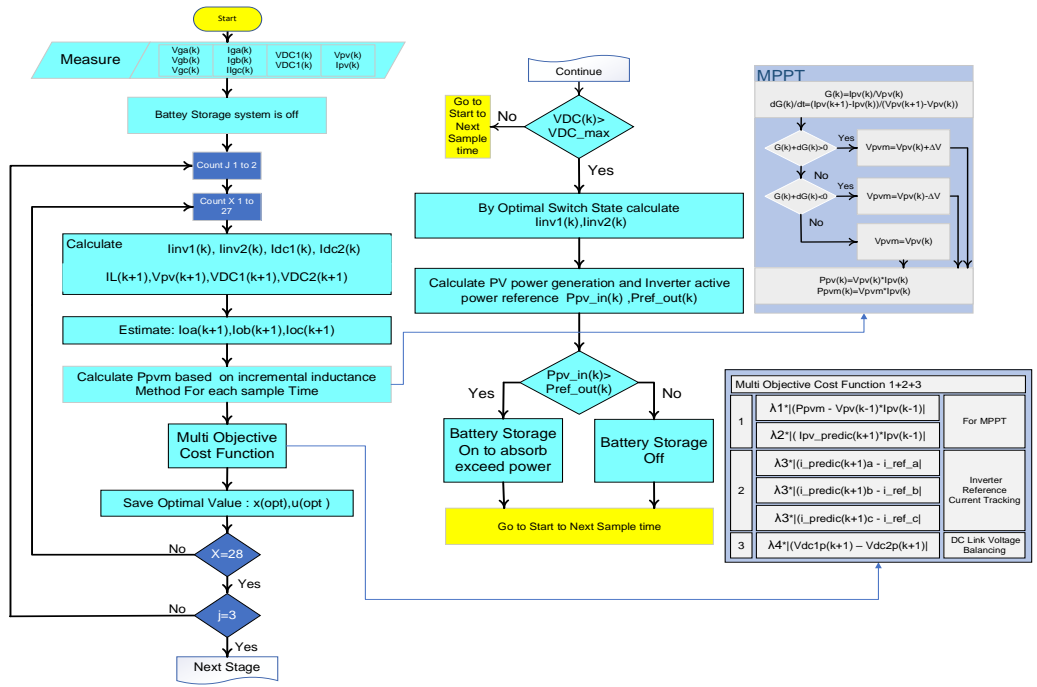


Fig. 6 Finite control set model predictive control proposed algorithm along with MPPT control

Table 2
The Simulation Parameters

The Simulation Parameters PV module name		Sun power
	-	•
Maximum power of module	[W]	305.226
Open circuit voltage Voltage of MPPT	[V]	64.2 54.7
-	[V]	
Parallel string	panel	66
Series connected module per string	series	5
Sun irradiance	[w/m²]	1000
Cell temperature	°C	25
Total nominal power	[kW]	100.7
Boost Converter & NPC Inverter		
C_{pv}	[uF]	1000
L_1, r_1	[mh], [m Ω]	5,5
C_{DC1} , C_{DC2}	[mF]	1.2,1.2
Frequency	[Hz]	60
VDC _{ref} , I _{nominal}	[V],[A]	500,370
LCL Filter		
Lf_1,Rf_1	[uH], [mΩ]	560 ,1
Lf_2,Rf_2	[uH], [mΩ]	440,1
Cf, Rf,	[uF], [Ω]	300,3
Three phase Grid		
Base voltage, V _{LL}	[V]	200
Short circuit level at base voltage	[MVA]	1
X/R ratio	-	7
Battery Storage, Buck Converter		
L_{B} , R_{B}	[mH], [mΩ]	2 ,5
Nominal Battery Voltage	[V]	96
Capacity	[AH]	500

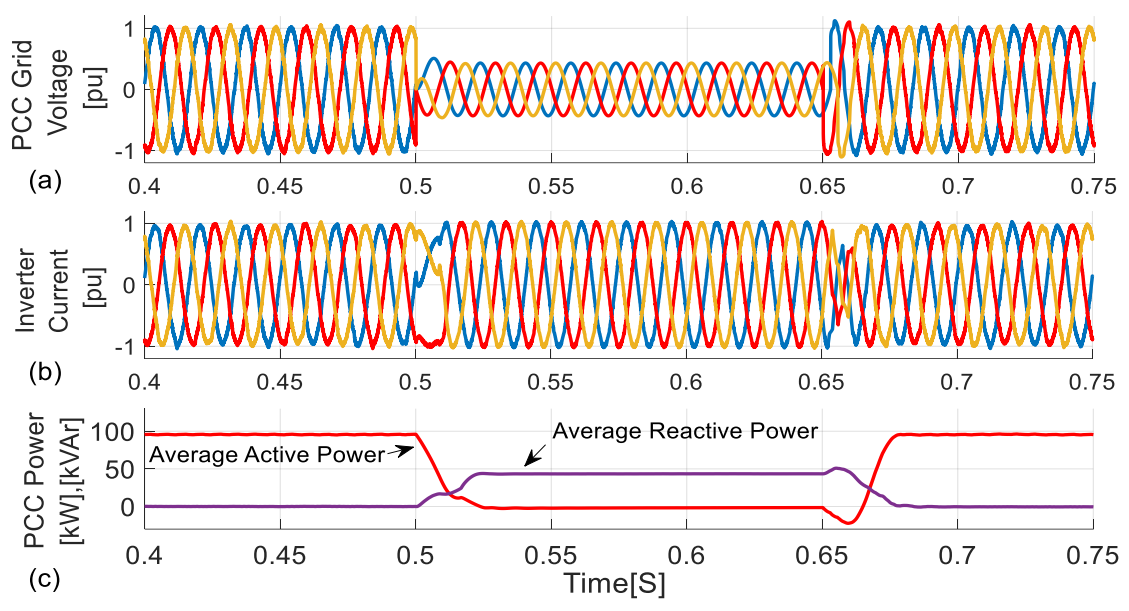


Fig. 7 Grid Fault Severe short circuit Three phases to the ground. (a) Grid Voltage. (b) Inverter Current. (c) Average active and reactive Power

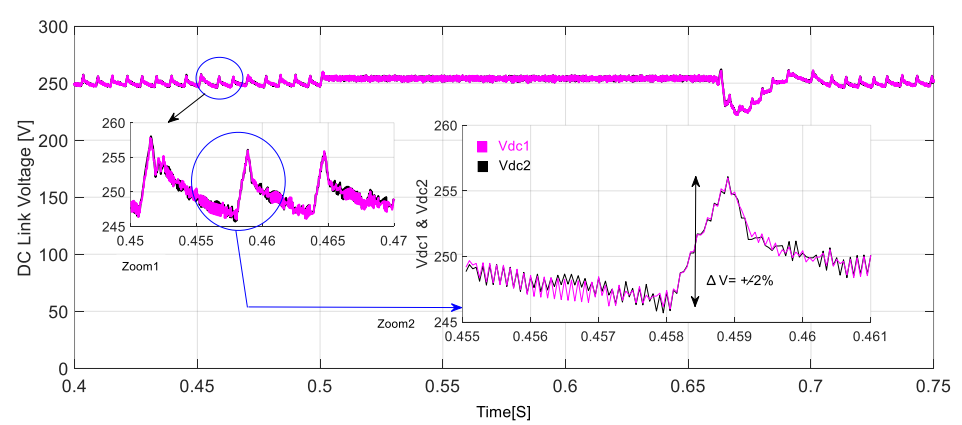


Fig. 8 DC Link Voltage control in normal and fault conditions

current produced by the photovoltaic array is approximately one per unit (base current is 370 A). In this scenario, from Fig. 7(a), a voltage drop of 50% has occurred in the PCC during 0.5 s to 0.65 s (Sobhy *et al.*, 2015). Symmetrical fault results in no negative sequence voltage being generated, but the amplitude of the positive sequence is reduced. The fault condition detector uses Eq. (26) and Fig. 5 to quickly detect this voltage sag in the PCC and subsequently calculates the reactive current reference according to Eq. (24). Then, the active current reference is calculated according to the maximum nominal current of the inverter and the reactive current reference.

In this article, maintaining the inverter current below its maximum allowed limit during grid fault is a priority. Fig. 7(b) and Fig. 7(c) show the inverter fault currents at about 400A and average active power at nearly zero value and reactive power injected at about 45 kVAr into the grid, respectively. Another objective of the control strategy is to maintain the MPPT function for the photovoltaic system, ensuring that power generation continues at its maximum value at about 100 kW. Due to reduced active power delivery to the grid, if the DC link voltage increases and reaches its maximum value at about 520 V, the control system activates the energy storage system and

absorbs all available excess power. This approach maintains the DC link voltage within its permissible range until the grid fault condition is cleared.

Figure 8 illustrates the voltage of the DC link capacitors under normal operating conditions and during grid fault conditions. The total measured voltage values of the DC link capacitors are compared to a reference value of 500 volts, with the resulting error converted into a positive current sequence component reference using the PI controller and the phase angle of the PLL. The multi-objective function of the proposed strategy selects the optimal state of the inverter switches by considering the voltage discrepancies among the capacitors in the DC link.

During normal operation, the voltage of the DC link capacitors in the NPC inverter is set at 250 V with a 4% ripple. When a three-line to-ground short-circuit grid fault occurs, the increase in capacitor voltage, along with the simultaneous presence of the fault, is managed using voltage sequence component separation in the control system. The on/off status of the boost converter switch, the states of the inverter switches, and the on/off status of the energy storage system switch are determined by the multi-objective function. As a result, each DC

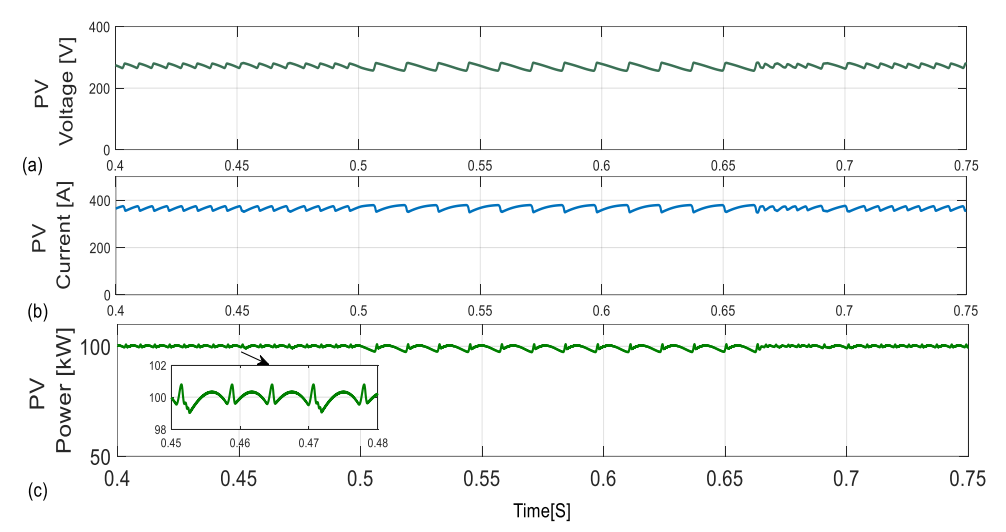


Fig. 9 Photovoltaic system control under three-phase symmetrical fault, (a) PV Voltage, (b) PV Current, (c) PV Power

link capacitor voltage remains balanced at approximately 250 volts, with no significant excess voltage or voltage drop in the DC link capacitors. While the generated PV power remains at MPPT, any generated power that is not delivered to the grid is directed to the energy storage system.

Fig. 9(a) shows the PV voltage curve and Fig. 9(b) shows the PV working current curve. Fig. 9(c) shows the PV output power, demonstrating that the proposed control strategy based on FCS-MPC has successfully implemented the MPPT algorithm(Ahmed *et al.*, 2022). When the grid fault occurs, the reactive power is injected into the grid and active power injection drops to zero. Meanwhile, the maximum power is absorbed from the PV panels at about 100 kW. This extra power – which is not injected into the grid – is stored in the BESS.

4.2 Low voltage ride through in the fault condition of a double line to ground short circuit fault

In this situation, a voltage imbalance is expected to occur at the PCC, resulting in the presence of positive sequence, negative sequence, and zero sequence voltages. The reference for the inverter current control is chosen to ensure that the current only contains the positive sequence term. Under this

condition, the inverter current is kept symmetrical sinusoidal without any over-current during fault and within the permissible range. Fig. 10 illustrates this situation. According to Fig. 10(a), the voltage at the PCC has dropped in two phases by 60% at t=0.5 s to 0.65 s. The current injected into the grid is completely sinusoidal with a positive sequence term of 400 A, as shown in Fig. 10(b). This is due to the presence of a negative sequence voltage at the PCC, Double frequency oscillations have appeared on the instantaneous active and reactive powers(Huka *et al.*, 2018).

In this condition, the reactive current is first injected according to the positive sequence grid voltage drop. Then, according to (24), with the remaining capacity of the inverter, the active current is injected into the grid up to the point that the total current of the inverter reaches its nominal value of 400 A. The references of reactive and active currents are set to 320 A and -237 A, respectively.

According to Fig. 10(b), the actual active and reactive currents well follow the reference values all in accordance with the theoretical analysis given in section 3.C. During LVRT, if the generated power from the PV panels is more than the active power delivered to the grid, the excess power is directed to the BESS. As a result, the DC link voltage of the inverter remains within the determined range.

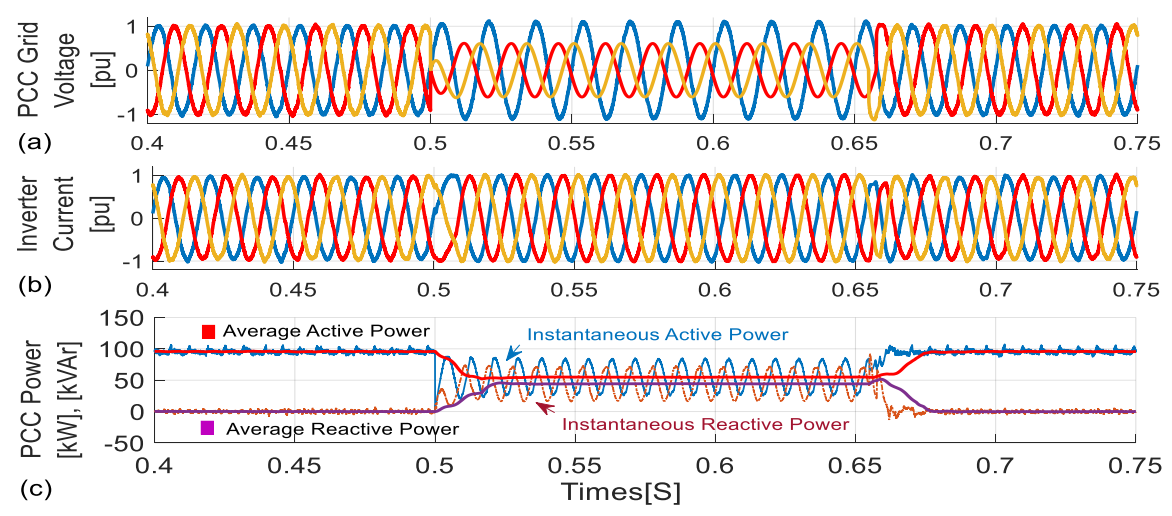


Fig 10. LVRT under double phase to ground fault, (a) PCC voltage, (b) Inverter output current, (c) Instantaneous and average Active, Reactive powers

4.3. Low voltage ride through in the fault condition of a single-phase to ground

In this case, two phases are healthy, and one phase experiences a voltage drop due to a grid fault. After detecting the fault, the reactive current reference is selected according to (24) so that the sum of the active and reactive currents does not exceed the inverter's permissible current limit. If the power generation of the photovoltaic system exceeds the power transmitted by the inverter, the voltage of the DC link is likely to increase beyond its normal operating limit of approximately 520V. By recognizing this issue through the control strategy, the energy storage system absorbs this excess energy. Fig. 11 shows the simulation results in this case. Fig. 11(a) shows the voltage drop of the PCC by 45 % in phase *a*.

The proposed control strategy ensures that the current injected into the grid remains sinusoidal, as shown in Fig. 11(b). With the reduction of the positive sequence of the PCC voltage, the reactive current is injected into the grid in proportion to the amount of voltage drop, as described by Eq. (24). In this case, the reactive current reference is set to -160 A. The remaining capacity of the inverter current is dedicated to injecting active current with the reference value of 366 A. In fault conditions, where the photovoltaic system operates at (MPPT), any excess power not injected into the grid is directed towards the energy storage system, similar to previous cases. Fig. 11(c) illustrates the active and reactive powers. During grid fault, the average active and reactive powers injected into the grid are 71.5 kW and 35 kVAr, respectively.

Fig. 12 compares the voltages and currents of the photovoltaic (PV) system and the boost converter under double-phase-to-ground and single-phase-to-ground short circuit conditions. In Fig. 12(a), the capacitors in the DC link of the NPC inverter are well balanced at 253 V, exhibiting a 5.5% ripple during the grid fault, which validates the performance of the proposed control strategy(4.2% as reported by (Monfared *et al.*, 2022)).

Table 3 presents the electrical parameters of the double and single-phase-to-ground short-circuit grid-connected PV system. Regarding Table 3, the upper and lower capacitor voltages in the DC link indicate that the upper capacitor voltage registers a peak of 262 V during fault conditions while maintaining a minimum voltage of 243 V, which reflects effective voltage regulation. The difference in upper capacitor voltage ($\Delta V_{\rm dc1}$) between the maximum and minimum values is 19 V. In contrast, the lower capacitor voltage also demonstrates stability, with a

maximum of 262 V and a minimum of 248 V, resulting in a voltage difference (ΔV_{dc2}) of 14 V. The stability of these voltage levels is critical for the overall performance of the system, ensuring that the DC link voltage remains within operational limits to support the inverter and PV system.

For Fig. 12(b), about the double-phase fault, the PV output voltage is 273 V with a 9.2% ripple, while Fig. 12(c) indicates that the PV output current is 365 A with an 8.2% ripple under fault conditions. In the case of the single-phase fault, as shown in Fig. 12(b), the PV output voltage remains at 273 V with a 9% ripple, while the PV output current also remains at 365 A with an 8% ripple under fault conditions as demonstrated in Fig. 12(c). Consequently, the PV-generated power maintains a value of 99.63 kW with a 2.3% ripple at the Maximum Power Point (MPP) as illustrated in Fig. 12(d).

According to Table 3, during normal operation, the phase voltages (Va, Vb, and Vc) remain stable at 117.8 V. However, under single-phase-to-ground (1LG) fault conditions, the phase voltage Vc drops to 65 V, while Vb decreases to 67 V during double-phase-to-ground (2LG) conditions. Furthermore, fluctuations in both positive and negative-sequence currents remain within acceptable limits, which is critical for ensuring system stability.

In terms of photovoltaic (PV) power generation, the system consistently outputs 100.8 kW during normal operation, with only minor fluctuations noted during fault conditions, recording 100.8 kW in 2LG and 101 kW in 1LG. Moreover, the BESS absorbs 0 kW during normal operations—indicating it does not engage in energy storage—its contribution becomes apparent during faults, absorbing 15.7 kW during the 1LG fault and increasing to 42 kW during the 2LG fault. Reactive power is injecting 28.9 kVAr during the 1LG fault and increasing to 45 kVAr during the 2LG fault. This reactive power injection is crucial for voltage support, enhancing the overall stability of the system during disturbances.

The MPPT functionality demonstrates effective performance across different operating states, with the MPPT output reaching 100.8 kW under normal conditions, closely aligning with the system's total PV power generation. Even under fault conditions, the MPPT system maintains consistency, peaking at 100.7 kW in 1LG and sustaining 100.8 kW in 2LG. Finally, the stability of the inductor current within the boost converter across various fault conditions indicates a continuous conduction mode (CCM) performance and a well-designed system capable of mitigating disturbances within the PV system.

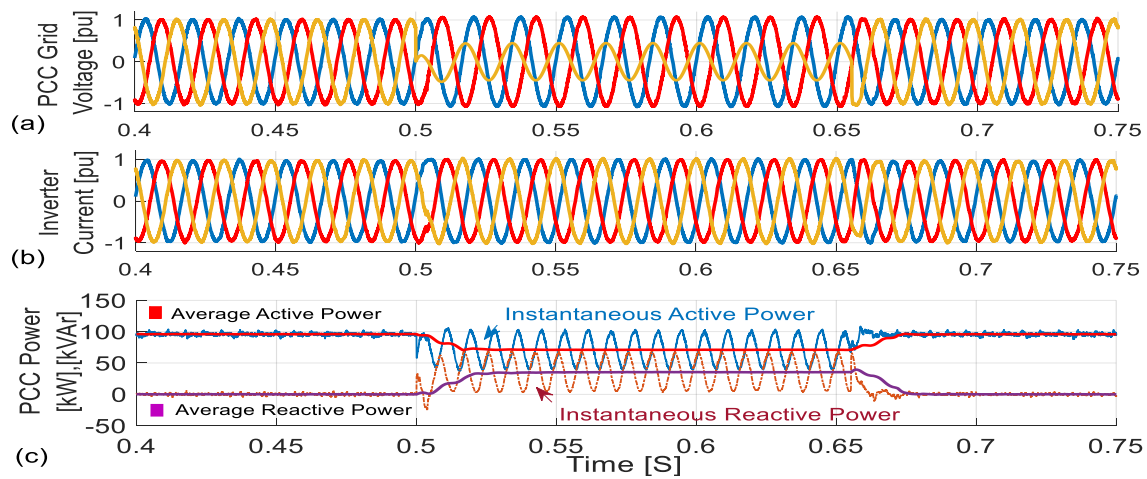


Fig. 11 LVRT under single phase to ground fault, (a) PCC voltage, (b) inverter output current, (c) instantaneous and average active and reactive powers

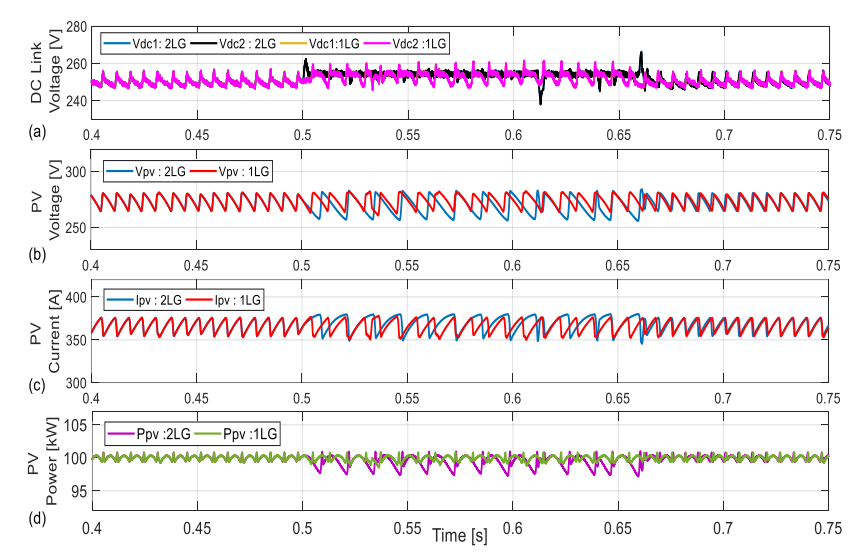


Fig. 12 Photovoltaic system control under Single-phase to ground fault(1LG) and double-phase to ground fault(2LG), (a) DC Link Voltages, (b) PV Voltages, (c) PV Currents, (d) PV Powers

Table 3

Double and single phase to ground short circuit electrical parameters of grid connected PV system

parameter	quantity	unit	Normal operation Values	2LG	1LG
PCC Voltage	$\begin{matrix} V_a \\ V_b \\ V_c \end{matrix}$	[V]	117.8 117.8 117.8	127 67 67	123 123 65
J	$V_{ m positive} \ V_{ m negative} \ V_{ m zero}$	[pu]	1.014 0.0 0.0	0.690 0.269 0.267	0.850 0.259 0.258
PCC Current	$I_{ m Line}$ $I_{ m positive}$ $I_{ m negative}$ $I_{ m zero}$	[A] [pu]	380 0.99 0.005 0	400 1.06 0.01 0	400 1.05 0.007 0
PCC Power	$P_{ m active}$	[kW] [kVAr]	96 0	53.4 45	79.8 28.9
Energy storage	P_{storage}	[kW]	0	42	15.7
Upper capacitor DC link voltage	$\max_{ ext{min}} \ \Delta V_{ ext{dc1}}$	[V]	256 246 10	262 248 14	262 243 19
Lower capacitor DC link voltage	$_{ m min} \ _{ m \Delta V_{ m dc2}}$	[V]	256 248 8	262 248 14	262 243 19
PV voltage	$\max _{ ext{min}} \ \Delta V_{pv}$	[V]	280 265 15	282 264 17	283 257 26
PV Current	$\max \ min \ \Delta I_{pv}$	[A]	375 354 21	380 351 29	379 350 29
PV Power generation	max min ΔPpv	[kW]	100.8 99.4 1.4	100.8 98.5 1.4	101 97.5 3.5
inductor current Boost converter	$\begin{array}{c} \text{max} \\ \text{min} \\ \Delta I_L \end{array}$	[A]	378 338 40	382 332 50	380 334 46

This comprehensive analysis underscores the robustness and efficiency of the grid-connected PV system both under normal operation and during the 1LG and 2LG fault scenarios.

4.4. Evaluation of the system operation under reduced power generation of the photovoltaic system and the voltage sag of the PCC

When photovoltaic (PV) power production decreases due to factors such as reduced radiation intensity or partial shading,

the input power to the inverter may fall below its output power. This discrepancy can lead to the discharge of the DC-link capacitor, resulting in a reduction of its voltage(Mohamed *et al.*, 2019). To address this issue, an effective control strategy must be implemented to maintain the DC-link voltage within permissible limits and prevent excessive voltage drop.

As shown in Fig. 13(a), before 0.5 seconds, the PCC grid voltage is stable, however, at 0.4 seconds the power generation of the PV system is reduced by approximately 50%.

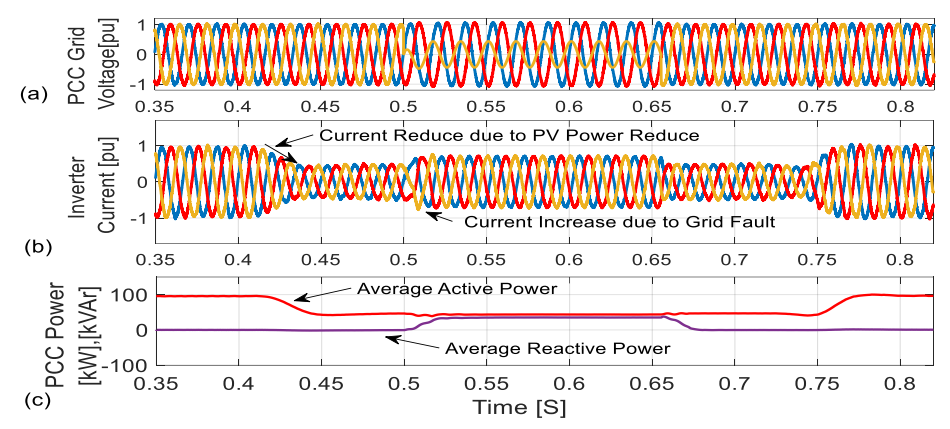


Fig. 13 The effect of reducing the intensity of light radiation and simultaneously single-phase fault

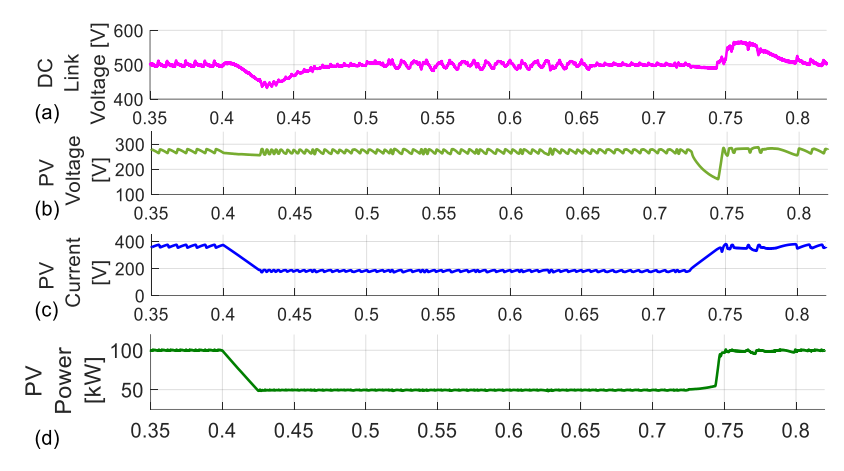


Fig. 14 DC-link and PV system control in the case of reduced light radiation and single phase grid fault, (a) DC-link voltage, (b) PV voltage, (c) PV current, (d) PV power

Consequently, according to Fig. 13(b), the control strategy adjusts the current reference from 1 per unit to 0.5 per unit to ensure the delivery of PV power, the inverter current is also reduced to 50%. As a result, the active power of the inverter is approximately 50 kW, while the reactive power is set to zero, as shown in Fig. 13(c).

During this reduction in PV power, the DC-link voltage illustrated in Fig. 14(a), decreases from around 500 V to 450 V due to the energy reduction. The PV voltage remains relatively unchanged (Fig. 14(b)), while the PV current decreases to 180 A (Fig. 14(c)), corresponding to a drop in PV power generation to 50 kW.

At t = 0.5 seconds, a single-phase grid fault causes a voltage drop of 55%, as indicated in Fig. 13(a). Upon detection of the fault, the reactive current reference is adjusted from 0 to -166 A using Eq. (24) to comply with grid code requirements, and the reactive power changes from 0 to 35 kVAr, as shown in Fig. 13(c). To enhance the LVRT capability under these conditions, the control strategy adjusts the active current reference to 228 A using Eq. (29) instead of Eq. (27). This ensures that the DC-link voltage does not fall below the nominal value, as demonstrated in Fig. 14(a). Additionally, Fig. 14(b) shows that the PV voltage remains at 272 V, while Fig. 14(c) indicates that the PV current decreases from 365 A to 182 A due to reduced radiation intensity, as illustrated in Fig. 14(d). The photovoltaic system continues to operate at its new maximum power point (Katche *et al.*, 2023).

According to Fig. 13(a), the grid fault is cleared at 0.65 seconds, prompting the reactive power injection reference to be reset to zero, returning to the pre-fault values. The active current reference is also adjusted to supply power under these conditions, with no use of BESS since there is no excess power. At 0.75 seconds and thereafter, the PV system's power gradually increases to its maximum normal operation of about 100 kW. To restrict the rise in DC-link voltage, which experiences a temporary spike to 550 V for 15 ms, the current reference rapidly increases from 0.5 per unit to 1 per unit to facilitate power delivery by the inverter. This evaluation indicates that the proposed strategy performs effectively across multiple objective functions.

4.5. A comparison of features in recent literature

The proposed method in this study is compared with recent methodologies across various research efforts, as summarized in Table 4. The goal of this comparison is to highlight the efficacy and comprehensiveness of our approach concerning LVRT capabilities in grid-connected PV systems.

Table 4 illustrates a variety of strategies employed in recent literature, such as (Zahloul *et al.*, 2024), who introduced a forward control strategy for enhanced LVRT capability, and (Smith *et al.*, 2024), who focused on using MPC techniques in three-level neutral-point clamped inverters under unbalanced grid conditions. The diversity of approaches demonstrates the ongoing innovation in the field of PV system control, with each

Table 4

Comparing the features of recent literature

N*	Reference	objective	strategy
		LVRT capability and stability analysis of an	
1	(Zahloul <i>et al.</i> , 2024)	advanced control approach based on voltage source converters	Fed-forward control
2	(Smith et al., 2024)	Improve the LVRT capability of a 3-level NPC inverter using MPC under unbalanced grid conditions.	Utilize an MPC algorithm for inverter control.
3	(Talha et al., 2022)	Design a multi-functional PV inverter with LVRT capability and constant power output.	Utilize a single-phase inverter with LVRT and low-irradiation compensation With feed-forward linearization
		Enhance the LVRT capability of grid-connected	1-Non-MPPT DC-link Voltage Control.
4	(Mohamed <i>et al.</i> , 2019)	photovoltaic systems by controlling the DC-link voltage.	2-Utilize an anti-windup technique in the PI controller.
		Improve the LVRT capability of grid-connected	1-Utilize a crowbar protection scheme in the
5	(Haidar & Julai, 2019)	photovoltaic systems to meet the requirements of	DC-link.
		grid codes.	2-Modify the reactive power control scheme.
c	(H-1 - / 1 0010)	Improve the LVRT capability of grid-connected	1-Utilize a PI-based current controller.
6	(Huka <i>et al.</i> , 2018)	photovoltaic systems under balanced and	2-Utilize an inner model control technique for
		unbalanced fault conditions.	DC-link voltage regulation
7	This paper	FCS-MPC for LVRT enhancement in grid-connected PV systems	Utilize a multi-objective MPC algorithm

N: Reference number

Table 5

Evaluating the existence of other effective parameters in PV system performance

Reference	MPPT under LVRT	DC Link Reactive power injection		LVRT and Low irradiation
number	WITT GRACE EVICE	balance	settling time	support
1	No	No	30 ms	No
2	No	Yes	30 ms	No
3	No	No	-	No
4	Yes	No	50 ms	No
5	No	No	25 ms	No
6	No	No	22 ms	No
7	Yes	Yes	20 ms	Yes

study offering unique insights into enhancing system resilience during voltage sags.

Our analysis reveals that successful control strategies must simultaneously address various operational goals. These include not only MPPT but also maintaining DC-link voltage stability, voltage balancing across capacitors, and adherence to grid-related active and reactive power injection requirements. For example, studies by (Mohamed *et al.*, 2019) and (Haidar & Julai, 2019) emphasize the necessity of enhancing DC-link voltage control and employing anti-windup techniques or crowbar protection schemes to better meet grid codes. In contrast, our proposed method uniquely incorporates a multi-objective FCS-MPC algorithm that allows for adaptive control of both reactive power injection and active power, ensuring optimal performance even under challenging fault conditions.

In addition to the capability to handle unbalanced and deep fault situations, our method excels in scenarios where environmental conditions can change unexpectedly—specifically in cases of low solar irradiation or potential shading. This feature significantly contributes to overall system reliability and maintains efficiency during and after grid faults. As indicated in Table 5, our methodology supports MPPT under LVRT conditions, which is critical for maintaining energy output and improving the return on investment for PV systems(Huka *et al.*, 2018).

Moreover, the incorporation of energy storage solutions further enhances our system's performance, allowing it to sustain power output near the MPP under various operational scenarios, thus improving its economic viability (Talha et al., 2022). The settling time for reactive power injections is

optimized to only 20 ms in our approach, outperforming several other identified methodologies, which can take up to 50 ms. This rapid response time aids in minimizing voltage fluctuations and enhancing the quality of current injected back into the grid (Mohamed *et al.*, 2019).

Furthermore, our results align well with previous works in the literature that emphasize the importance of adaptive current reference adjustments. Controlling active and reactive power injections in real-time, as proposed by(Haidar & Julai, 2019), can lead to improved system responses during grid disturbances. This is critical for compliance with modern grid codes. The ability of our method to perform effectively during both LVRT conditions and low irradiation support reinforces the significance of a resilient design in advanced PV inverter systems.

In conclusion, by synergizing various control strategies and incorporating real-time adaptive responses, our proposed method demonstrates notable improvements over existing techniques in enhancing LVRT capabilities. This underscores an essential trend in photovoltaic technology toward more integrated, resilient systems capable of meeting the challenges posed by modern electric grid demands.

5. Conclusion

This article presents a novel control strategy based on FSC-MPC to enhance the LVRT capability of grid-connected photovoltaic system based on NPC inverter. The proposed method determines the optimal switching state from 54 possible

combinations, taking into account the inverter output currents control, DC link voltage control, voltage balance of the two DC link capacitors in NPC, and (MPPT). To realize the mentioned goals, a multi-objective cost function is developed to control both the boost converter and NPC inverter, ensuring the photovoltaic system operates in MPPT mode during lowvoltage conditions, thereby minimizing power losses and operation. Simulation in ensuring safe MATLAB/Simulink environment demonstrate that the proposed LVRT control strategy offers the following advantages,

- During grid fault, the over-current in the inverter output current is avoided the current is well limited to the maximum allowable value. Also, it is kept sinusoidal without any negative-sequence term during grid fault. Furthermore, the actual current well follows the reference value.
- 2) The reactive current is injected into the faulty grid in accordance with the LVRT grid codes. With the remaining capacity of the inverter, the active current/power is injected into the grid.
- The DC-link voltage of the NPC inverter is controlled at its reference value and over-voltage and voltage drop are avoided during grid fault.
- 4) The balance of capacitor voltages is maintained which is an important challenge in NPC inverters during unbalanced grid conditions.
- 5) Notably, the MPPT strategy is implemented through the cost function which eliminates the need to define the duty cycle for the boost converter. The extra active power generated by PV panels during grid faults is stored in the energy storage system.

It should be noted that in the proposed LVRT strategy, all the control objectives are included in a multi-objective MPC that provides a fast dynamic response which is of importance during grid faults.

Author Contributions: All authors have read and agreed to the published version of the manuscript.

Funding: The authors received no financial support for the research, authorship, and/or publication of this article.

Conflicts of Interest: The authors declare no conflict of interest.

References

- Abdelsalam, A. K., Massoud, A. M., Ahmed, S., & Enjeti, P. N. (2011). High-performance adaptive perturb and observe MPPT technique for photovoltaic-based microgrids. *IEEE Transactions on Power Electronics*, 26(4), 1010-1021. https://doi.org/10.1109/tpel.2011.2106221
- Abramovitz, A., & Smedley, M. (2012). Survey of solid-state fault current limiters. *IEEE Transactions on Power Electronics*, 27(6), 2770-2782. https://doi.org/10.1109/tpel.2011.2174804
- Afshari, E., Moradi, G. R., Rahimi, R., Farhangi, B., Yang, Y., Blaabjerg, F., & Farhangi, S. (2017). Control strategy for three-phase grid-connected PV inverters enabling current limitation under unbalanced faults. *IEEE Transactions on industrial electronics*, 64(11), 8908-8918. https://doi.org/10.1109/tie.2017.2733481
- Ahmed, M., Harbi, I., Kennel, R., Rodríguez, J., & Abdelrahem, M. (2022). Maximum power point tracking-based model predictive control for photovoltaic systems: Investigation and new

- perspective. Sensors, 22(8), 3069. https://doi.org/10.3390/s22083069
- Al-Shetwi, A. Q., Hannan, M., Jern, K. P., Alkahtani, A. A., & PG Abas, A. (2020). Power quality assessment of grid-connected PV system in compliance with the recent integration requirements. *Electronics*, 9(2), 366. https://doi.org/10.3390/electronics9020366
- Al-Shetwi, A. Q., & Sujod, M. Z. (2018). Grid-connected photovoltaic power plants: A review of the recent integration requirements in modern grid codes. *International Journal of Energy Research*, 42(5), 1849-1865. https://doi.org/10.1002/er.3983
- Alam, M. S., Abido, M., Hossain, M. I., Choudhury, M. S. H., & Uddin, M. A. (2018). Series dynamic braking resistor based protection scheme for inverter based distributed generation system. 2018 International Conference on Innovations in Science, Engineering and Technology (ICISET), https://doi.org/10.1109/ICISET.2018.8745629
- Alrubaie, A. J., Al-Khaykan, A., Malik, R., Talib, S. H., Mousa, M. I., & Kadhim, A. M. (2022). Review on MPPT Techniques in Solar System. 2022 8th International Engineering Conference on Sustainable Technology and Development (IEC), https://doi.org/10.1109/IEC54822.2022.9807500
- Anagreh, Y. N., Alnassan, A., & Radaideh, A. (2021). High Performance MPPT Approach for Off-Line PV System Equipped With Storage Batteries and Electrolyzer. *International Journal of Renewable Energy Development*, 10(3). https://doi.org/10.14710/ijred.2021.34131
- Asghar, R., Rehman, F., Ullah, Z., Aman, A., Iqbal, K., & Ali Nawaz, A. (2020). Modified switch type fault current limiter for low-voltage ride-through enhancement and reactive power support of DFIG-WT under grid faults. *IET Renewable Power Generation*, 14(9), 1481-1490. https://doi.org/10.1049/iet-rpg.2019.1058
- Camacho, A., Castilla, M., Miret, J., Borrell, A., & de Vicuña, L. G. (2014). Active and reactive power strategies with peak current limitation for distributed generation inverters during unbalanced grid faults. *IEEE Transactions on industrial electronics*, 62(3), 1515-1525. https://doi.org/10.1109/TIE.2014.2347266
- Castilla, M., Miret, J., Sosa, J. L., Matas, J., & de Vicuña, L. G. (2010). Grid-fault control scheme for three-phase photovoltaic inverters with adjustable power quality characteristics. *IEEE Transactions on Power Electronics*, 25(12), 2930-2940. https://doi.org/10.1109/TPEL.2010.2070081
- Chen, H.-C., Lee, C.-T., Cheng, P.-T., Teodorescu, R., & Blaabjerg, F. (2016). A low-voltage ride-through technique for grid-connected converters with reduced power transistors stress. *IEEE Transactions on Power Electronics*, 31(12), 8562-8571. https://doi.org/10.1109/TPEL.2016.2522511
- Djilali, L., Sanchez, E. N., Ornelas-Tellez, F., Avalos, A., & Belkheiri, M. (2019). Improving microgrid low-voltage ride-through capacity using neural control. *IEEE Systems Journal*, 14(2), 2825-2836. https://doi.org/10.1109/JSYST.2019.2947840
- Donoso, F., Mora, A., Cardenas, R., Angulo, A., Saez, D., & Rivera, M. (2017). Finite-set model-predictive control strategies for a 3L-NPC inverter operating with fixed switching frequency. *IEEE Transactions on industrial electronics*, 65(5), 3954-3965. https://doi.org/10.1109/TIE.2017.2760840
- Dursun, M., & DÖŞOĞLU, M. K. (2018). LCL filter design for grid connected three-phase inverter. 2018 2nd International Symposium on Multidisciplinary Studies and Innovative Technologies (ISMSIT), https://doi.org/10.1109/ISMSIT.2018.8567054
- Farrokhabadi, M., Cañizares, C. A., Simpson-Porco, J. W., Nasr, E., Fan, L., Mendoza-Araya, P. A., Tonkoski, R., Tamrakar, U., Hatziargyriou, N., & Lagos, D. (2019). Microgrid stability definitions, analysis, and examples. *IEEE Transactions on Power Systems*, 35(1), 13-29. https://doi.org/10.1109/TPWRS.2019.2925703
- Gulalkari, M., & Chaudhary, M. (2020). Control Technique with Integrated Low Voltage Ride Through Capability and Anti-Islanding in Grid Connected Inverter. 2020 IEEE First International Conference on Smart Technologies for Power, Energy and Control (STPEC), https://doi.org/10.1109/STPEC49749.2020.9297734

- Haidar, A. M., & Julai, N. (2019). An improved scheme for enhancing the ride-through capability of grid-connected photovoltaic systems towards meeting the recent grid codes requirements. *Energy for Sustainable Development*, 50, 38-49. https://doi.org/10.1016/j.esd.2019.02.007
- Hassan, Z., Amir, A., Selvaraj, J., & Rahim, N. (2020). A review on current injection techniques for low-voltage ride-through and grid fault conditions in grid-connected photovoltaic system. *Solar Energy*, 207, 851-873. https://doi.org/10.1016/j.solener.2020.06.085
- Hossain, M. K., & Ali, M. H. (2014). Low voltage ride through capability enhancement of grid connected PV system by SDBR. 2014 IEEE PES T&D Conference and Exposition, https://doi.org/10.1109/TDC.2014.6863248
- Huka, G. B., Li, W., Chao, P., & Peng, S. (2018). A comprehensive LVRT strategy of two-stage photovoltaic systems under balanced and unbalanced faults. *International Journal of Electrical Power & Energy Systems*, 103, 288-301. https://doi.org/10.1016/j.ijepes.2018.06.014
- Ikaouassen, H., Raddaoui, A., Rezkallah, M., & Chandra, A. (2019). Real-time implementation of improved predictive model control for standalone power generation system based PV renewable energy. *IET Generation, Transmission & Distribution*, 13(7), 1068-1077. https://doi.org/10.1049/iet-gtd.2018.501
- Jacobson, M. Z., von Krauland, A.-K., Coughlin, S. J., Dukas, E., Nelson, A. J. H., Palmer, F. C., & Rasmussen, K. R. (2022). Low-cost solutions to global warming, air pollution, and energy insecurity for 145 countries [10.1039/D2EE00722C]. Energy & Environmental Science. https://doi.org/10.1039/D2EE00722C
- Jalili, K., & Bernet, S. (2009). Design of \$ LCL \$ filters of active-frontend two-level voltage-source converters. *IEEE Transactions on* industrial electronics, 56(5), 1674-1689. https://doi.org/10.1109/TIE.2008.2011251
- Jalilian, A., Hagh, M. T., Abapour, M., & Muttaqi, K. M. (2015). DC-link fault current limiter-based fault ride-through scheme for inverter-based distributed generation. *IET Renewable Power Generation*, *9*(6), 690-699. https://doi.org/10.1049/iet-rpg.2014.0289
- Jalilian, A., Naderi, S. B., Negnevitsky, M., & Hagh, M. T. (2018). Controllable DC-link bridge-type FCL for low voltage ride-through enhancement of converter interfaced DG systems. *International Journal of Electrical Power & Energy Systems*, 95, 653-663. https://doi.org/10.1016/j.ijepes.2017.09.022
- Katche, M. L., Makokha, A. B., Zachary, S. O., & Adaramola, M. S. (2023). A comprehensive review of maximum power point tracking (mppt) techniques used in solar pv systems. *Energies*, 16(5), 2206. https://doi.org/10.3390/en16052206
- Kerekes, T., Séra, D., & Máthé, L. (2017). Three-phase photovoltaic systems: structures, topologies, and control. In *Renewable Energy Devices and Systems with Simulations in MATLAB® and ANSYS®* (pp. 67-90). CRC Press. https://doi.org/10.1080/15325008.2015.1030518
- Lashab, A., Sera, D., Guerrero, J. M., Mathe, L., & Bouzid, A. (2017).

 Discrete model-predictive-control-based maximum power point tracking for PV systems: Overview and evaluation. *IEEE Transactions on Power Electronics*, 33(8), 7273-7287. https://doi.org/10.1109/TPEL.2017.2764321
- Lee, C.-T., Hsu, C.-W., & Cheng, P.-T. (2011). A low-voltage ridethrough technique for grid-connected converters of distributed energy resources. *IEEE Transactions on Industry Applications*, 47(4), 1821-1832. https://doi.org/10.1109/TIA.2011.2155016
- Lim, S., & Choi, J. (2015). LCL filter design for grid connected NPC type three-level inverter. *International journal of renewable energy research*, 5(1), 45-53.
- Lin, X., Han, Y., Yang, P., Wang, C., & Xiong, J. (2018). Low-voltage ride-through techniques for two-stage photovoltaic system under unbalanced grid voltage sag conditions. 2018 IEEE 4th Southern Power Electronics Conference (SPEC), https://doi.org/10.1109/SPEC.2018.8636016
- Liu, H., Xu, K., Zhang, Z., Liu, W., & Ao, J. (2019). Research on theoretical calculation methods of photovoltaic power shortcircuit current and influencing factors of its fault characteristics. *Energies*, 12(2), 316. https://doi.org/10.3390/en12020316
- Liu, Y., & Tian, L. (2016). Research on low voltage ride through technology of grid-connected photovoltaic system. 2016

- International Conference on Smart Grid and Clean Energy Technologies (ICSGCE), https://doi.org/10.1109/ICSGCE.2016.7876055
- Liu, Y., Wang, C. S., & Cao, Y. (2022). A Finite Control Set Model Predictive Control Algorithm for PV Maximum Power Point Tracking. 2022 9th International Forum on Electrical Engineering and Automation (IFEEA), https://doi.org/10.1109/IFEEA57288.2022.10037837
- Mahmoudi, H., Moamaei, P., Aleenejad, M., & Ahmadi, R. (2017). A new maximum power point tracking method for photovoltaic applications based on finite control set model predictive control. 2017 IEEE Applied Power Electronics Conference and Exposition (APEC), https://doi.org/10.1109/APEC.2017.7930834
- Miret, J., Castilla, M., Camacho, A., de Vicuña, L. G., & Matas, J. (2012). Control scheme for photovoltaic three-phase inverters to minimize peak currents during unbalanced grid-voltage sags. *IEEE Transactions on Power Electronics*, 27(10), 4262-4271. https://doi.org/10.1109/TPEL.2012.2191306
- Mirhosseini, M., Pou, J., & Agelidis, V. G. (2014). Single-and two-stage inverter-based grid-connected photovoltaic power plants with ride-through capability under grid faults. *IEEE Transactions on sustainable energy*, 6(3), 1150-1159. https://doi.org/10.1109/TSTE.2014.2347044
- Mohamed, S. R., Jeyanthy, P. A., Devaraj, D., Shwehdi, M., & Aldalbahi, A. (2019). DC-link voltage control of a grid-connected solar photovoltaic system for fault ride-through capability enhancement. *Applied Sciences*, *9*(5), 952. https://doi.org/10.3390/app9050952
- Monfared, K. K., Neyshabouri, Y., Iman-Eini, H., & Liserre, M. (2022).

 An improved finite control-set model predictive control for nested neutral point clamped converter. *IEEE Transactions on industrial electronics*, 70(6), 5386-5398. https://doi.org/10.1109/TIE.2022.3196337
- Mortazavian, S., Shabestary, M. M., & Mohamed, Y. A.-R. I. (2016). Analysis and dynamic performance improvement of grid-connected voltage–source converters under unbalanced network conditions. *IEEE Transactions on Power Electronics*, 32(10), 8134-8149. https://doi.org/10.1109/TPEL.2016.2633994
- Naderi, S. B., Davari, P., Zhou, D., Negnevitsky, M., & Blaabjerg, F. (2018). A review on fault current limiting devices to enhance the fault ride-through capability of the doubly-fed induction generator based wind turbine. *Applied Sciences*, 8(11), 2059. https://doi.org/10.3390/app8112059
- Naderi, S. B., Negnevitsky, M., Jalilian, A., Hagh, M. T., & Muttaqi, K. M. (2017). Low voltage ride-through enhancement of DFIG-based wind turbine using DC link switchable resistive type fault current limiter. *International Journal of Electrical Power & Energy Systems*, 86, 104-119. https://doi.org/10.1016/j.ijepes.2016.10.001
- Naresh, P., & Kumar, V. S. S. (2020). Analysis of low voltage ride through techniques for grid-connected photovoltaic systems. 2020 IEEE International Conference on Power Electronics, Smart Grid and Renewable Energy (PESGRE2020), https://doi.org/10.1109/PESGRE45664.2020.9070365
- Nezhad, A. A., Zaker, B., Arani, A. A. K., & Gharehpetian, G. (2017). Impact of non-MPPT operation mode of PV system considering inverter fault current limiting. 2017 Conference on Electrical Power Distribution Networks Conference (EPDC), https://doi.org/10.1109/EPDC.2017.8012739
- Nguyena, T. H., Dang, Q. V., Ngo, X. C., & Do, N. Y. (2023). Long-term performance of roof-top GCPV systems in central Viet Nam. *International Journal of Renewable Energy Development*, 12(6). https://doi.org/10.14710/ijred.2023.56569
- Omar, M. A., & Mahmoud, M. M. (2021). Improvement approach for matching pv-array and inverter of grid connected pv systems verified by a case study. *International Journal of Renewable Energy Development*, 10(4), 687. https://doi.org/10.14710/ijred.2021.36082
- Pant, S., & Saini, R. (2019). Comparative study of MPPT techniques for solar photovoltaic system. 2019 International Conference on Electrical, Electronics and Computer Engineering (UPCON), https://doi.org/10.1109/UPCON47278.2019.8980004
- RajaMohamed, S., Jeyanthy, P. A., Devaraj, D., & Bouzguenda, M. (2019). Performance comparison of active and passive LVRT strategies for grid connected PV systems. 2019 IEEE International

- Conference on Intelligent Techniques in Control, Optimization and Signal Processing (INCOS), https://doi.org/10.1109/INCOS45849.2019.8951327
- Rashid, G., & Ali, M. H. (2014). A modified bridge-type fault current limiter for fault ride-through capacity enhancement of fixed speed wind generator. *IEEE Transactions on Energy Conversion*, 29(2), 527-534. https://doi.org/10.1109/TEC.2014.2304414
- Rodriguez, F., Bueno, E., Aredes, M., Rolim, L., Neves, F. A., & Cavalcanti, M. C. (2008). Discrete-time implementation of second order generalized integrators for grid converters. 2008 34th Annual Conference of IEEE Industrial Electronics, https://doi.org/10.1109/IECON.2008.4757948
- Rodriguez, P., Luna, A., Munoz-Aguilar, R. S., Etxeberria-Otadui, I., Teodorescu, R., & Blaabjerg, F. (2011). A stationary reference frame grid synchronization system for three-phase grid-connected power converters under adverse grid conditions. *IEEE Transactions on Power Electronics*, 27(1), 99-112. https://doi.org/10.1109/TPEL.2011.2159242
- Rodríguez, P., Pou, J., Bergas, J., Candela, J. I., Burgos, R. P., & Boroyevich, D. (2007). Decoupled double synchronous reference frame PLL for power converters control. *IEEE Transactions on Power Electronics*, 22(2), 584-592. https://doi.org/10.1109/TPEL.2006.890000
- Romero-Cadaval, E., Spagnuolo, G., Franquelo, L. G., Ramos-Paja, C. A., Suntio, T., & Xiao, W. M. (2013). Grid-connected photovoltaic generation plants: Components and operation. *IEEE Industrial Electronics Magazine*, 7(3), 6-20. https://doi.org/10.1109/MIE.2013.2264540
- Rossi, M., Karamanakos, P., & Castelli-Dezza, F. (2022). An Indirect Model Predictive Control Method for Grid-Connected Three-Level Neutral Point Clamped Converters With \$ LCL \$ Filters. *IEEE Transactions on Industry Applications*, *58*(3), 3750-3768. https://doi.org/10.1109/TIA.2022.3152463
- Sadeghkhani, I., Golshan, M. E. H., Guerrero, J. M., & Mehrizi-Sani, A. (2016). A current limiting strategy to improve fault ride-through of inverter interfaced autonomous microgrids. *IEEE Transactions on Smart Grid*, 8(5), 2138-2148. https://doi.org/10.1109/TSG.2016.2517201
- Sadeghkhani, I., Hamedani Golshan, M. E., Mehrizi-Sani, A., & Guerrero, J. M. (2018). Low-voltage ride-through of a droop-based three-phase four-wire grid-connected microgrid. *IET Generation, Transmission & Distribution, 12*(8), 1906-1914. https://doi.org/10.1049/iet-gtd.2017.1306
- Safaei, A., Zolfaghari, M., Gilvanejad, M., & Gharehpetian, G. B. (2020).
 A survey on fault current limiters: Development and technical aspects. *International Journal of Electrical Power & Energy Systems*, 118, 105729. https://doi.org/10.1016/j.ijepes.2019.105729
- Singh, O., & Gupta, S. K. (2018). A review on recent Mppt techniques for photovoltaic system. 2018 IEEMA Engineer Infinite Conference (eTechNxT),
 - https://doi.org/10.1109/ETECHNXT.2018.8385315
- Smith, C., Gargoom, A., Arif, M. T., & Haque, M. E. (2024). Model predictive control of 3L-NPC inverter to enhance fault ride through capability under unbalanced grid conditions. *IET Power Electronics*. https://doi.org/10.1049/pel2.12754
- Sobhy, T., Hemdan, N., Hamada, M., & Wahab, M. (2015). German grid code aspects discussion: low voltage ride-through of converter

- based decentralized generation. Int. J. Distrib. Energy Resour. Smart Grids, 11, 129-141.
- Talha, M., Raihan, S. R. S., Abd Rahim, N., Akhtar, M. N., Butt, O. M., & Hussain, M. M. (2022). Multi-Functional PV Inverter With Low Voltage Ride-Through and Constant Power Output. *IEEE Access*, 10, 29567-29588. https://doi.org/10.1109/ACCESS.2022.3158983
- Teodorescu, R., Liserre, M., & Rodriguez, P. (2011). *Grid converters for photovoltaic and wind power systems*. John Wiley & Sons. https://doi.org/10.1002/9780470667057
- Troester, E. (2009). New German grid codes for connecting PV systems to the medium voltage power grid. 2nd International workshop on concentrating photovoltaic power plants: optical design, production, grid connection, https://www.researchgate.net/file.PostFileLoader.html?id=56fc d7b848954c26780b2de1&assetKey=AS:345608402554880@1459410872390
- Wang, Y., Yang, P., Yin, X., & Ma, Y. (2014). Evaluation of low-voltage ride-through capability of a two-stage grid-connected three-level photovoltaic inverter. 2014 17th International Conference on Electrical Machines and Systems (ICEMS), https://doi.org/10.1109/ICEMS.2014.7013598
- Wen, H., & Fazeli, M. (2019a). A low-voltage ride-through strategy using mixed potential function for three-phase grid-connected PV systems. *Electric Power Systems Research*, *173*, 271-280. https://doi.org/10.1016/j.epsr.2019.04.039
- Wen, H., & Fazeli, M. (2019b). A new control strategy for low-voltage ride-through of three-phase grid-connected PV systems. *The Journal of Engineering*, 2019(18), 4900. https://doi.org/10.1049/joe.2018.9254
- Xu, J., Xie, S., & Tang, T. (2013). Evaluations of current control in weak grid case for grid-connected LCL-filtered inverter. *IET Power Electronics*, 6(2), 227-234. https://doi.org/10.1049/iet-pel.2012.0192
- Yang, Y., Enjeti, P., Blaabjerg, F., & Wang, H. (2015). Wide-scale adoption of photovoltaic energy: Grid code modifications are explored in the distribution grid. *IEEE Industry Applications Magazine*, 21(5), 21-31. https://doi.org/10.1109/MIAS.2014.2345837
- Yu, F., Zhou, C., Liu, X., & Zhu, C. (2021). Model-free predictive current control for three-level inverter-fed IPMSM with an improved current difference updating technique. *IEEE Transactions on Energy Conversion*, 36(4), 3334-3343. https://doi.org/10.1109/TEC.2021.3069274
- Zahloul, H., Khaliq, A., Hamzehbahmani, H., Veremieiev, S., & Salous, S. (2024). Evaluation of LVRT capability and stability analysis of VSC based advanced control approach for grid connected PV system under grid fault conditions. *Heliyon*, 10(5). https://doi.org/10.1016/j.heliyon.2024.e26935
- Zeb, K., Islam, S. U., Khan, I., Uddin, W., Ishfaq, M., Busarello, T. D. C., Muyeen, S., Ahmad, I., & Kim, H. (2022). Faults and Fault Ride Through strategies for grid-connected photovoltaic system: A comprehensive review. *Renewable and Sustainable Energy Reviews*, 158, 112125. https://doi.org/10.1016/j.rser.2022.112125



© 2025. The Author(s). This article is an open access article distributed under the terms and conditions of the Creative Commons Attribution-ShareAlike 4.0 (CC BY-SA) International License (http://creativecommons.org/licenses/by-sa/4.0/)